Short Papers

Analytical Solutions for the Radiated Emission of Parallel Microstrip Traces

Bin-Chyi Tseng, Li-Chun Liao, Lin-Kun Wu, *Member, IEEE*, and Hui-Tsui Lung

***Abstract*—A closed-form expression of the unintentional electromagnetic radiation of parallel microstrip traces is proposed. Based on transmission line theory, far-field Green's function, and concept of array factor in antenna theory, analytical solutions for the electric field radiated from a pair of parallel microstrip lines are developed. Depending on the printed circuit board material, dimension parameters, and termination impedances, the frequency and angular responses of far-field radiated emission on the upper half-plane can be analyzed by the presented method. The differential- and common-mode radiated emission solutions are validated by a full-wave simulator and test board measurements in a full-anechoic chamber.**

***Index Terms*—Crosstalk, Green function, microstrip, printed circuits.**

I. Introduction

Rapid advances in science and technology in recent years have led to increased requirements for high-speed data transmission. Since data rates are directly proportionate to the bandwidth and carrier frequency [1], in modern circuit systems, large numbers of high-speed interconnections are routed in parallel on printed circuit boards (PCB). For electromagnetic coupled parallel signal traces, the crosstalk that exists between traces is problematic and plays an important role in determining the performance of circuit systems. An enclosure is usually applied to attenuate the coupling field. Due to the random switching patterns on each line, a single trace will reveal both velocity and impedance changes that also affect system performance. Moreover, with the lowering of supply voltage for high-frequency circuits, unintentional radiation, which interferes with other circuits, is becoming a major problem in a novel circuit design [2], [3].

In high-speed data communication, differential signaling (e.g., IEEE1394b, USB3.0, etc.), which inherently exhibits better immunity to noise, has found increasing applications. However, when the differential signal is imbalanced in phase or amplitude, a common-mode current will be introduced on the traces [4], [5]. Generally, the common-mode current is the dominant source for noise emission [6]. But, due to the square relation between emission and operating frequency of a differential-mode current [7], we should take both the common- and differential-mode current into consideration for high-frequency applications.

This paper presents closed-form solutions for common- and differential-mode radiation of a pair of parallel microstrip traces. Based on the concept of array factor in antenna theory and Green's functions for the metal-backed dielectric layer [8], the far-field radiated emissions of parallel traces, depending on the PCB's material, dimension parameters, and termination impedance, are calculated. The presented differential- and common-mode radiated emission solutions are verified by a full-wave simulator and practical test board measurements in a full-anechoic chamber.

Manuscript received September 20, 2010; revised February 15, 2011; accepted March 20, 2011. Date of publication May 19, 2011; date of current version August 18, 2011. This work was supported by the National Science Council, Taiwan, R.O.C., under Grant 98-2221-E-035-025.

B.-C. Tseng is with the Department of Electrical Engineering, Feng Chia University, Taichung, Taiwan 40724, R.O.C. (e-mail: bctseng@ieee.org).

L.-C. Liao is with the Department of Computer Science and Information Engineering, Chaoyang University of Technology, Taichung, Taiwan 41349, R.O.C. (e-mail: lcliao@cyut.edu.tw).

L.-K. Wu and H.-T. Lung are with the Institute of Communication Engineering, National Chiao Tung University, Hsinchu, Taiwan 30050, R.O.C. (e-mail: lkwu@cc.nctu.edu.tw; htlung@cc.nctu.edu.tw).

Digital Object Identifier 10.1109/TEMC.2011.2136344

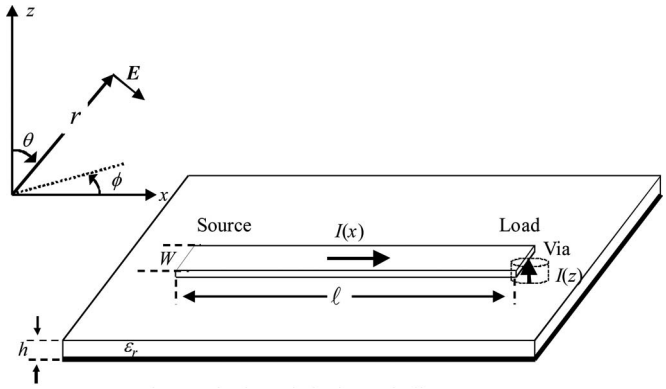

Fig. 1. Single-ended microstrip line structure.

II. Analytical Solutions

A. Single-Ended Transmission Line

The radiated electric field of a conductor, with surface current density J_S on a surface S, is expressed as follows:

$$\boldsymbol{E}(\boldsymbol{r}) = \int_S J_s(r')\overline{\boldsymbol{G}}(\boldsymbol{r},\boldsymbol{r}')\,d\boldsymbol{S} \tag{1}$$

where $\overline{G}$ is the dyadic Green's function of various radiation structures. For a microstrip line structure with source and load at two terminals, as shown in Fig. 1, currents exist on the microstrip line in the x-direction and on the via in the z-direction. Assuming that the ground plane and the dielectric layer extend in the x- and y-directions infinitely, the far-field Green's function of a unit dipole in the x-direction is given by [9]

$$\boldsymbol{G}_x = \frac{j\omega\mu_0}{4\pi}\frac{e^{-jk_0 r}}{r}\boldsymbol{F}_x \tag{2}$$

with

$$\boldsymbol{F}_x = (R_v - 1)(\cos\theta\cos\phi)\,\boldsymbol{e}_\theta + (R_h + 1)(\sin\phi)\,\boldsymbol{e}_\phi \tag{3}$$

where

$$R_v = \frac{1 - j\frac{v}{\varepsilon_r\cos\theta}\tan(k_0 vh)}{1 + j\frac{v}{\varepsilon_r\cos\theta}\tan(k_0 vh)}$$

$$R_h = \frac{1 + j\frac{v}{\cos\theta}\cot(k_0 vh)}{1 - j\frac{v}{\cos\theta}\cot(k_0 vh)}$$

and $\quad v = \sqrt{\varepsilon_r - \sin^2\theta}.$

In (3), $\boldsymbol{e}_\theta$ and $\boldsymbol{e}_\phi$ are the unit vectors in spherical coordinates. Up to 1 GHz, the dielectric losses are not significant. When the dielectric thickness h is much less than the operating wavelength, that is $k_0 h \ll 1$, the tangent and cotangent functions in R_v and R_h can be simplified. So, $\boldsymbol{F}_x$ is reduced to

$$\boldsymbol{F}_x \approx 2jk_0 h\left[\left(\frac{\sin^2\theta}{\varepsilon_r} - 1\right)(\cos\phi)\,\boldsymbol{e}_\theta + (\cos\theta\sin\phi)\,\boldsymbol{e}_\phi\right].$$

In the z direction, the dyadic Green's function of the via is

$$\boldsymbol{G}_z = \frac{j\omega\mu_0}{4\pi}\cos(k_0 v z')\frac{e^{-jk_0 r}}{r}\boldsymbol{F}_z. \tag{4}$$

Similarly, as $k_0 h \ll 1$, $\boldsymbol{F}_z$ results in

$$\boldsymbol{F}_z \approx \frac{2\sin\theta}{\varepsilon_r}\boldsymbol{e}_\theta. \tag{5}$$

In practical PCB designs, the signal trace follows the quasi-TEM condition, so the surface current distribution $I(x)$ can be approximated as a line current. Also, because of the extremely thin substrate, the current variation in the z-direction can be ignored. Therefore, (1) is replaced by

$$\begin{aligned}\boldsymbol{E}(\boldsymbol{r}) = &\int_{x'=0}^{x'=\ell} I(x')\boldsymbol{G}_x e^{jk_0\boldsymbol{r}'\cdot\boldsymbol{e}_r}dx' \\ &+\int_{z'=-h}^{z'=0}\boldsymbol{G}_z I(0)e^{jk_0\boldsymbol{r}'\cdot\boldsymbol{e}_r}dz' \\ &-\int_{z'=-h}^{z'=0}\boldsymbol{G}_z I(\ell)e^{jk_0\boldsymbol{r}'\cdot\boldsymbol{e}_r}dz'\end{aligned} \tag{6}$$

where $\boldsymbol{e}_r$ is the unit vector in the r-direction of spherical coordinates. Therefore,

$$\boldsymbol{r}'\cdot\boldsymbol{e}_r = x'\sin\theta\cos\phi + z'\cos\theta.$$

Combining (2), (4), and (6), the radiated electric field integration in (1) results in

$$\begin{aligned}\boldsymbol{E}(\boldsymbol{r}) = \frac{j\omega\mu_0}{4\pi}\frac{e^{-jk_0 r}}{r}\Bigg\{&\boldsymbol{F}_x\int_{x'=0}^{x'=\ell} I(x')e^{jk_x x'}dx' \\ &+\boldsymbol{F}_z\int_{z'=-h}^{z'=0}\left[I(0)-I(\ell)e^{jk_x\ell}\right]\cos(k_0 v z')e^{jk_z z'}dz'\Bigg\}\end{aligned} \tag{7}$$

where

$$\begin{aligned}k_x &= k_0\sin\theta\cos\phi \\ k_z &= k_0\cos\theta.\end{aligned}$$

With the same condition, $k_0 h \ll 1$, the second integral term of (7) simplifies to

$$\int_{z'=-h}^{z'=0}\cos(k_0 v z')e^{jk_z z'}dz' \approx h.$$

By the general transmission line theorem, the current distribution $I(x)$ on a trace is

$$I(x) = \frac{V_S}{Z_S+Z_C}\frac{1}{1-\rho_S\rho_L e^{-j\beta 2\ell}}\left(e^{-j\beta x}-\rho_L e^{-j\beta 2\ell}e^{j\beta x}\right) \tag{8}$$

where V_S is the excitation voltage, Z_S and Z_C are the impedance of signal source and transmission line, respectively, and ρ_S and ρ_L are the reflection coefficients at source and load, respectively.

Finally, we obtain the far-field radiation of a single-ended microstrip line with arbitrary terminal load [8]

$$\begin{aligned}\boldsymbol{E}(\boldsymbol{r}) = &\frac{\omega\mu_0}{4\pi}\frac{e^{-jk_0 r}}{r}\frac{V_S}{Z_S+Z_C}\frac{1}{1-\rho_S\rho_L e^{-j\beta 2\ell}} \\ &\times\Bigg\{\boldsymbol{F}_x\left[\frac{1-e^{-j(\beta-k_x)\ell}}{\beta-k_x}+\rho_L e^{-j\beta 2\ell}\frac{1-e^{j(\beta+k_x)\ell}}{\beta+k_x}\right] \\ &+jh\boldsymbol{F}_z\left[1-\rho_L e^{-j\beta 2\ell}-(1-\rho_L)e^{-j(\beta-k_x)\ell}\right]\Bigg\}.\end{aligned} \tag{9}$$

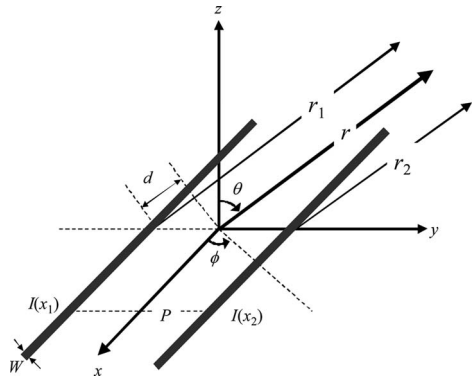

Fig. 2. Differential transmission line structure.

B. Differential Pair Transmission Lines

A differential transmission line structure is demonstrated in Fig. 2. As we can see in this constitution, there are two identical single-ended microstrip line elements separated by the distance P. When the current in each line is the same as that of an isolated one (i.e., the mutual coupling is neglected), the differential-mode current can be described as [7]

$$\begin{aligned}I(x_1) &= I_D \\ I(x_2) &= -I_D.\end{aligned} \tag{10}$$

Combining these current functions into (9), the total far-field radiation of a differential-mode current is

$$\begin{aligned}\boldsymbol{E}(\boldsymbol{r}) = &\frac{\omega\mu_0}{4\pi}\left(\frac{e^{-jk_0 r_1}}{r_1}-\frac{e^{-jk_0 r_2}}{r_2}\right) \\ &\times\frac{V_S}{Z_S+Z_C}\frac{1}{1-\rho_S\rho_L e^{-j\beta 2\ell}} \\ &\times\Bigg\{\boldsymbol{F}_x\left[\frac{1-e^{-j(\beta-k_x)\ell}}{\beta-k_x}+\rho_L e^{-j\beta 2\ell}\frac{1-e^{j(\beta+k_x)\ell}}{\beta+k_x}\right] \\ &+jh\boldsymbol{F}_z\left[1-\rho_L e^{-j\beta 2\ell}-(1-\rho_L)e^{-j(\beta-k_x)\ell}\right]\Bigg\}.\end{aligned} \tag{11}$$

The relations between r_1, r_2, and r, are $r_1 = r + d$ and $r_2 = r - d$ with

$$d = \left(\boldsymbol{e}_x\frac{P}{2}\right)\cdot\boldsymbol{e}_r = \frac{P}{2}\sin\theta\sin\phi. \tag{12}$$

For a far-field observation, $d \ll r$, we can obtain the following simplified result:

$$\begin{aligned}\frac{e^{-jk_0 r_1}}{r_1}-\frac{e^{-jk_0 r_2}}{r_2} &= \frac{e^{-jk_0(r+d)}}{r+d}-\frac{e^{-jk_0(r-d)}}{r-d} \\ &\approx \frac{e^{-jk_0 r}}{r}\left(e^{-jk_0 d}-e^{jk_0 d}\right).\end{aligned} \tag{13}$$

By using the pattern multiplication method [10], the total radiation of a pair of parallel microstrip traces is given by the following relation:

$$\boldsymbol{E}_{\text{total}}(\boldsymbol{r}) = \text{AF}\times\boldsymbol{E}(\boldsymbol{r})$$

where AF is the array factor with

$$\text{AF} = e^{jk_0 d}\pm^{-jk_0 d}.$$

For a differential signal, the array factor has the form

$$\text{AF}_{\text{DM}} = e^{jk_0 d}-e^{-jk_0 d} = 2j\sin(k_0 d). \tag{14}$$

With this array factor, the total far-field radiation of a pair of parallel microstrip traces driven by a differential-mode current is

$$\boldsymbol{E}_{\mathrm{DM}}(\boldsymbol{r}) = 2j\sin(k_0 d)\times\frac{e^{-jk_0 r}}{r} \times\frac{\omega\mu_0}{4\pi}\frac{V_S}{Z_S+Z_C}\frac{1}{1-\rho_S\rho_L e^{-j\beta 2\ell}} \times\left\{\boldsymbol{F}_x\left[\frac{1-e^{-j(\beta-k_x)\ell}}{\beta-k_x}+\rho_L e^{-j\beta 2\ell}\frac{1-e^{j(\beta+k_x)\ell}}{\beta+k_x}\right] +jh\boldsymbol{F}_z\left[1-\rho_L e^{-j\beta 2\ell}-(1-\rho_L)e^{-j(\beta-k_x)\ell}\right]\right\}. \quad (15)$$

For a common-mode signal, the current distribution can be written as

$$I(x_1) = I(x_2) = I_C. \quad (16)$$

Similarly, the array factor is

$$\mathrm{AF}_{\mathrm{CM}} = e^{jk_0 d} + e^{-jk_0 d} = 2\cos(k_0 d). \quad (17)$$

So, the total far-field radiation of a pair of parallel microstrip traces driven by a common-mode current is formulated by

$$\boldsymbol{E}_{\mathrm{CM}}(\boldsymbol{r}) = 2\cos(k_0 d)\times\frac{e^{-jk_0 r}}{r} \times\frac{\omega\mu_0}{4\pi}\frac{V_S}{Z_S+Z_C}\frac{1}{1-\rho_S\rho_L e^{-j\beta 2\ell}} \times\left\{\boldsymbol{F}_x\left[\frac{1-e^{-j(\beta-k_x)\ell}}{\beta-k_x}+\rho_L e^{-j\beta 2\ell}\frac{1-e^{j(\beta+k_x)\ell}}{\beta+k_x}\right] +jh\boldsymbol{F}_z\left[1-\rho_L e^{-j\beta 2\ell}-(1-\rho_L)e^{-j(\beta-k_x)\ell}\right]\right\}. \quad (18)$$

III. Results

Using the analytical results achieved in Section II, the single-end, common- and differential-mode radiated emission can be quickly obtained. To confirm the analytical result of a single-ended microstrip line, a full-wave, 3-D method of moments-based simulator EMSIM (IBM, Yorktown Heights, NY) was utilized. As a first example, a microstrip line structure with excitation source $V_S = 1$ V and shorted termination load (i.e., $\rho_L = -1$) was performed. The line width $W = 0.7$ mm, trace length $\ell = 100$ mm, substrate thickness $h = 0.4$ mm, dielectric constant $\varepsilon_r = 4.4$, and copper thickness $t = 17.8$ μm are the parameters used to simulate and fabricate a test board. With the designed characteristic impedance $Z_C = 50\ \Omega$ and assigned source impedance $Z_S = 50\ \Omega$, the radiated electric field at 3 m with $\theta = \phi = 0^\circ$ is calculated and demonstrated in Fig. 3. As demonstrated in [2] and [11], the correspondence between the analytical result and the full-wave simulation result is good.

To further validate the results between numerical solutions and measurement, the radiation power of the test board in a 9 m × 6 m × 6 m full-anechoic chamber is measured. With the same conditions as applied in numerical simulations, the radiated electric field, which is converted from the measured radiation power, is also depicted in Fig. 3. At 800 MHz, the λ/2 resonance is observed in the perpendicular direction for all three methods.

Following the developed estimation method for a parallel microstrip lines is confirmed. Fig. 4 shows the configurations for numerical simulations and measurement. To evaluate the emission effectiveness of differential signaling, the same substrate material and board size (i.e., $N = 300$ mm) used in the single-ended case are applied. Due to the electromagnetic coupling between parallel traces, the width of a 50 Ω microstrip line is modified from 0.7 to 0.68 mm and separated by spacing $S = 0.9$ mm [12].

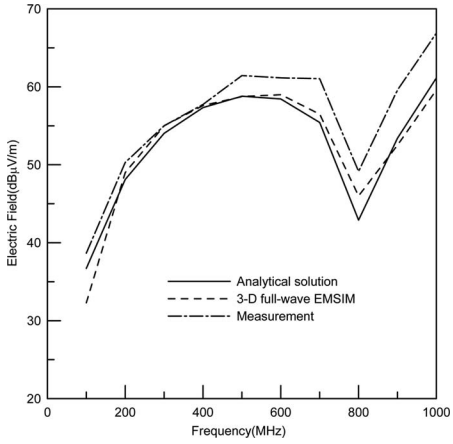

Fig. 3. Comparison of a single-ended transmission line.

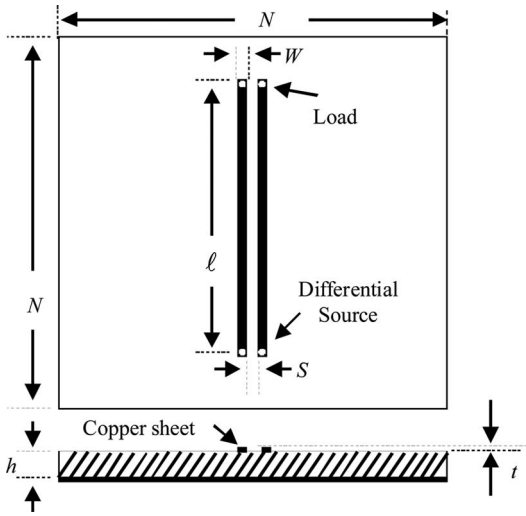

Fig. 4. Top and cross-sectional view of differential pair structure.

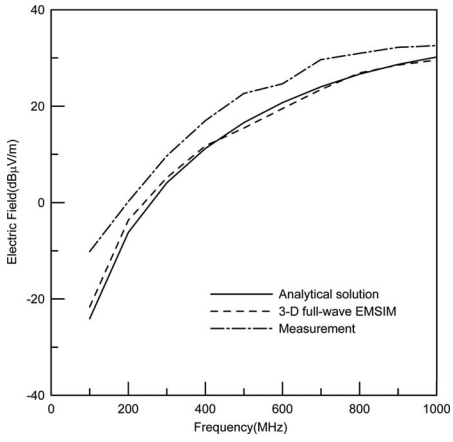

Fig. 5. Comparison of differential transmission lines.

In a matched condition (i.e., $\rho_L = 0$), the numerical results that come from the full-wave electromagnetic simulator and those from our analytical solution at $\theta = 45^\circ$, $\phi = 90^\circ$, and $r = 3$ m are both illustrated in Fig. 5. With the same procedure, the test board is measured and its results are also displayed in Fig. 5. As we can see in this comparison,

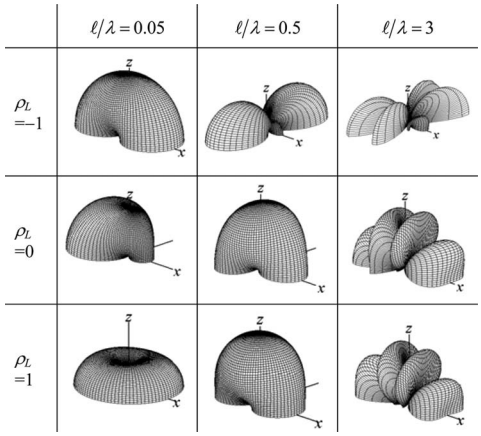

Fig. 6. Radiation patterns of a parallel coupled common-mode traces for different trace lengths and loading conditions.

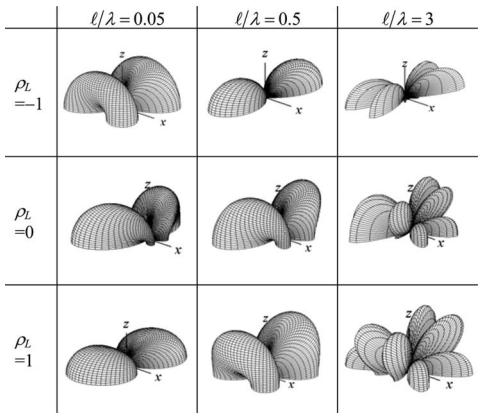

Fig. 7. Radiation patterns of a parallel coupled differential-mode traces for different trace lengths and loading conditions.

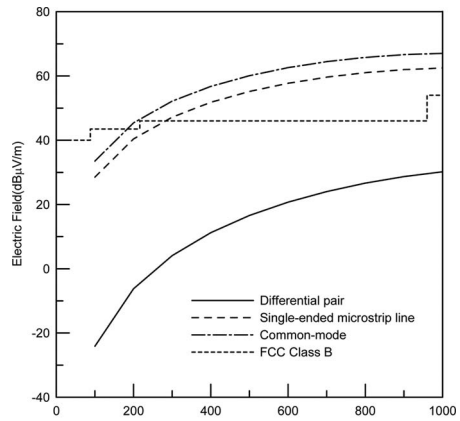

Fig. 8. Comparison of various transmission lines.

the correspondence between the proposed estimation method and full-wave simulation is good. But, due to the diffraction effect at the board edge, the measured data are larger than those from the analytical results.

As a demonstration of various radiation patterns of the parallel coupled common- and differential-mode traces, Figs. 6 and 7 show the 3-D diagrams for three different line lengths $\ell/\lambda = 0.05$, 0.5, 3, and loading conditions $\rho_L = -1$, 0, and 1. The radiation patterns are calculated according to (15) and (18). As can be seen in Fig. 6, the common-mode radiation patterns are similar to those of a single trace in [8]. For differential-mode radiation patterns depicted in Fig. 7, all the 3-D diagrams have nulls in the perpendicular x–z cutting plane (i.e., $y = 0$) as expected. When the trace length is a multiple of wavelength, the radiation patterns exhibit complex side lobes under various loading conditions.

With these validated analytical solutions, the single-ended, common- and differential-mode circuits are driven with an equal excitation magnitude. At the same observation point, $\theta = 45°$, $\phi = 90°$, and $r = 3$ m, the superior emission cancellation effect of differential signaling is noted and the square relation between emission and operating frequency of a differential-mode current is observed in Fig. 8. As frequency increases, the differential-mode radiation increases more rapidly than common-mode current radiation.

IV. Conclusion

In high-speed interconnections, differential signaling schemes have found increasing applications. In this paper, the unintentional electromagnetic radiation of the parallel structure is formulated by using array factor. When this approximated function is applied to a circuit board with finite size, the diffraction effect at the edge is ignored. With the developed far-field analytical solutions, the radiated emission on the upper half-plane, depending on the PCB's material, dimension parameters, and termination impedance, can be determined easily and quickly. From the validated results, the radiated emission of a differential pair is much lower than that of the single-ended transmission line. Using these closed-form expressions, a high-speed circuit designer can evaluate the radiation effect of a parallel structure and modify the design to meet electromagnetic compatibility regulations.

References

[1] A. C. Scogna and F. Zanella, "Broadband signal integrity characterization of a high speed differential backplane pair," in *Proc. IEEE Int. Symp. Electromagn. Compat.*, vol. 1, Aug. 2006, pp. 24–28.

[2] S. Daijavad, J. Janak, H. Heeb, A. Ruehli, and D. McBride, "A fast methodfor computing radiation from printed circuit boards," *Proc. IEEE Int. Symp. Electromagn. Compat.*, Aug. 1990, pp. 300–304.

[3] K. Naishadham, J. B. Berry, and H. A. N. Hejase, "Full-wave analysis of radiated emission from arbitrarily shaped printed circuit traces," *IEEE Trans. Electromagn. Compat.*, vol. 35, no. 3, pp. 366–377, Aug. 1993.

[4] B. C. Tseng and L. K. Wu, "Design of miniaturized common-mode filter by multilayer low-temperature co-fired ceramic," *IEEE Trans. Electromagn. Compat.*, vol. 46, no. 4, pp. 571–579, Nov. 2004.

[5] K. B. Hardin and C. R. Paul, "Decomposition of radiating structures using the ideal structure extraction methods (ISEM)," *IEEE Trans. Electromagn. Compat.*, vol. 35, no. 2, pp. 264–273, May 1993.

[6] S. Daijavad, B. , and J. Rubin, "Modeling common-mode radiation of 3-D structures," *IEEE Trans. Electromagn. Compat.*, vol. 34, no. 1, pp. 57–61, Feb. 1992.

[7] C. R. Paul, *Introduction to Electromagnetic Compatibility*, 2nd ed. New York: Wiley, 2006, ch. 8.

[8] M. Leone, "Closed-form expressions for the electromagnetic radiation of microstrip signal traces," *IEEE Trans. Electromagn. Compat.*, vol. 49, no. 2, pp. 322–328, May 2007.

[9] D. A. Hill, D. G. Camell, K. H. Cavcey, and G. H. Koepke, "Radiated emissions and immunity of microstrip transmission lines:Theory and reverberation chamber measurements," *IEEE Trans. Electromagn. Compat.*, vol. 38, no. 2, pp. 165–172, May 1996.

[10] C. A. Balanis, *Antenna Theory*. New York: Wiley, 1996, ch. 6.

[11] B. J. Rubin and S. Daijavad, "Radiation andscattering from structures involving finite-size dielectric regions," *IEEE Trans. Antennas Propag.*, vol. 38, no. 11, pp. 1863–1873, Nov. 1990.

[12] D. M. Pozar, *Microwave Engineering*, 3rd ed. New York: Wiley, 2005, pp. 337–347.